Research on Multi-Objective Aerodynamic/Structural Design Optimization Method for Large Thickness Flatback Airfoils

Kang-yuan Zhou*[1,2], Shi-qiang Zhang*[3], Wen-Ping Song*[1,2], Jian-Hua Xu [1,2], Zhong-Hua Han [1,2]

[1]School of Aeronautics, Northwestern Polytechnical University, Xi'an 710071, P. R. China
[2]National Key Laboratory of Aircraft Configuration Design, Xi'an 710072, P. R. China
[3]Jilin Chongtong Chengfei New Material Co., LTD., Chongqing, 401336, China
*These authors contribute equally to this paper

Abstract

With the operation of ultra-large wind turbines exceeding 10 MW, the blade length has significantly increased. Further consideration is needed for the contribution of the root airfoil family (with a relative thickness >40%) to improve the wind energy capture capacity of wind turbines and meet the structural constraint requirements. The large-thickness flatback airfoils offer advantages such as a larger slope of the lift curve, a higher maximum lift coefficient, and better structural characteristics. These advantages contribute to blade weight reduction and performance improvement, making it a preferable choice for balancing both aerodynamic and structural requirements. However, flatback airfoils that have not been designed with good compromises may incur severe drag penalties and fail to improve both blade structural performance and aerodynamic performance. This paper presents a multi-objective aerodynamic/structural design optimization for large-thickness flatback airfoil. The method takes the minimization of airfoil drag at the design state as the aerodynamic performance optimization objective, and maximize the sum of the cross-sectional stiffnesses of the airfoil profile in the flapwise and edgewise directions as the structural performance optimization objective. The validity of the optimization framework is verified through the aerodynamic and structural optimization of a flatback airfoil with a relative thickness of 60%, resulting in a set of 25 optimal shapes from the Pareto solution. Considering that the accuracy limitation of the rapid aerodynamic performance evaluation method used in the optimization design in predicting the aerodynamic characteristics of airfoils with large blunt trailing edge separation flow, the aerodynamic characteristic comparison of the optimized airfoil and the baseline is carried out by using a high-fidelity IDDES method. For the optimized airfoil with the most balanced aerodynamic and structural performances, the drag coefficient at the design state is reduced by 33.79%, the cross-section flapwise stiffness is increased by 16.0%, and the cross-section edgewise stiffness is increased by 9.4%, verifying the effectiveness of the multi-objective design optimization method developed in this paper. Moreover, the numerical simulation results obtained by the high-fidelity IDDES method are further analyzed to reveal the physical mechanisms of the aerodynamic performance improvements of the optimized airfoil presented in this paper.

Keywords: Large-thickness flatback airfoil, Multi-objective design optimization, Aerodynamic/Structural, IDDES

1. General Introduction

According to the Global Wind Energy Council (GWEC)[1], the world is expected to add 680GW of installed wind power capacity between 2023 and 2027, of which 130GW will come from offshore wind. This figure shows that the wind power industry is still growing rapidly and that offshore wind will play an increasing role. However, the global offshore wind energy development is becoming increasingly saturated, offshore wind power to the deep sea, large-scale development of the trend is becoming more and more obvious. Currently offshore wind turbine giant enterprises Vestas, Siemens, China Ming Yang Group, China Shanghai Electric and other newly developed large-scale offshore wind turbines have reached more than 15MW single capacity[2], the blade spread length of more than 120m, such as the Ming Yang Group's ultra-large-scale offshore wind turbine MySE292, which impeller

diameter of 292m, the length of the blade reaches 143m[3]. The increase in blade length means that the distance between the large-thickness airfoil at the root (relative thickness >40%) and the paddle hub further increases, and its aerodynamic performance becomes more and more important in terms of its impact on the blade's ability to capture wind energy, which needs to be further developed in order to improve its contribution to wind energy capture capability while meeting structural constraints.

This kind of large thickness airfoil has a significant cross-sectional area and moment of inertia, which better meets the structural strength requirements of wind turbine blades and contributes to weight reduction. However, it exhibits a stronger inverse pressure gradient compared to thin airfoils, leading to more intense flow separation, significantly decreasing aerodynamic performance. This makes it challenging to be directly applied to the design of large wind turbines. The flatback design can help alleviate this issue. Research by Sandia National Laboratories in the U.S. indicates that[4][5], compared to conventional thick airfoils, flatback airfoils further improve the cross-sectional area and moment of inertia, reduce the inverse pressure gradient on the suction surface, and slow down the separation of the boundary layer. This enhancement benefits both structural characteristics and lift performance.

However, the design of large thickness flatback airfoils still faces many difficulties, such as: (1) Although the flatback design is conducive to the improvement of lift and structural characteristics, the consequent trailing edge vortex shedding brings about a drag penalty. Flatback airfoils that are not designed with an optimal compromise may increase the drag penalty caused by the trailing edge, which in turn leads to a decrease in the lift-to-drag ratio[6]. Balancing lift and drag is one of the major challenge in the design of flatback airfoils. (2) Most flatback airfoils are obtained from conventional airfoils by trailing edge trimming. For example, van Dam et al.[7][8] used direct truncation and symmetric thickening to obtain flatback airfoils, which are used in the design of large wind turbine blades. These methods can conveniently and quickly produce flatback airfoils but often cannot achieve optimal structural and aerodynamic performance. (3) The aerodynamic characteristics of flatback airfoils exhibit strong three-dimensional effects and non-constant behavior due to the influence of trailing edge vortex shedding. The commonly used RANS method struggles to accurately evaluate their aerodynamic characteristics, while the LES method requires significant time and resources. This presents a challenge for both the design process and the evaluation of results.

Aiming at these difficulties, this paper focuses on minimizing airfoil drag under the design state as the aerodynamic performance optimization objective and maximizing the sum of the cross-sectional stiffnesses of the airfoil profile in the flapwise and edgewise directions as the structural performance optimization objective. The research involves the development of a design optimization methodology by using a multi-objective optimization algorithm based on a surrogate model. The optimization process employs MSES software with a basic drag correction to balance the efficiency and accuracy in calculating aerodynamic performance. Considering that the accuracy limitation of the rapid aerodynamic performance evaluation method used in the optimization design in predicting the aerodynamic characteristics of airfoils with large blunt trailing edge separation flow, the aerodynamic characteristic comparison of the optimized airfoil and the baseline is carried out by using a high-fidelity IDDES method. The results from the high-fidelity evaluation are then used to perform a mechanism analysis.

The first part of this paper is an introductory section that includes the need for the development of large thickness flatback airfoils and their advantages and disadvantages. The second part describes the geometrical parameterization method, aerodynamic/structural performance evaluation method and numerical optimization method used. In the third part, the performance of the airfoil before and after optimization is evaluated comparatively, and the physical mechanism of its performance improvement is analyzed. The last part summarizes the work of this paper.

2. Methodology

2.1 Geometric parameterization method

In this paper, the CST (Class Function/Shape Function Transformation) parameterization method is selected for the optimization design of large thickness flatback airfoils. This parameterization method, proposed by Kulfan[9], is based on the transformation of class and shape functions and can accurately describe the geometrical shape of the airfoil. It shows promising application prospects in the

aerodynamic optimization of wind turbine airfoils.

The parameterized expressions for the geometric perturbations of the upper and lower surfaces of the airfoil using the CST parameterization method are as follows:

$$\begin{aligned} y_s &= C(x)\cdot S_s(x) + x\cdot y_{TEs} \\ y_p &= C(x)\cdot S_p(x) + x\cdot y_{TEp} \end{aligned} \tag{1}$$

where the subscripts ‘s’ and ‘p’ represent the suction surface and pressure surface surfaces of the airfoil. C(x) is the class function shown in Eq.(2); and S(x) is the shape function, which is often defined as the superposition of the Bernstein polynomials shown in Eq.(3).

$$C(x) = x^{N1}\cdot(1-x)^{N2} \tag{2}$$

$$\begin{aligned} S_s(x) &= \sum_{i=0}^{N} A_{si}\cdot S_i(x) \\ S_p(x) &= \sum_{i=0}^{N} A_{pi}\cdot S_i(x) \\ S_i(x) &= \frac{N!}{i!(N-i)!}x^i(1-x)^{N-i} \end{aligned} \tag{3}$$

where ‘N’ is the order of parameterization, ‘N1’ and ‘N2’ are parameters that determine the type of geometry, the ‘A_{si}’ and ‘A_{pi}’ are the weight coefficients for each Bernstein polynomial, which can be obtained by applying the least square method on the airfoil’s points.

2.2 Assessment methodology and validation

2.2.1 Rapid Assessment Method of Aerodynamic Performance and Validation

In order to improve the efficiency of the optimization, MSES[10] with the base drag correction is used in this paper to evaluate the aerodynamic performance during the design optimization. The commonly used base drag estimation formula for flatback airfoils is shown in Eq. (4), which is obtained by F. Grasso[11] through modifying the formula of Hoerner[12], which expresses the base drag coefficient through a function of the drag coefficient (Cd) and the dimensionless trailing edge thickness (h).

$$\Delta C_{dbase,0} = 0.135\cdot h^{4/3} / C_d^{1/4} \tag{4}$$

This correction formula is not suitable for large thickness wind turbine airfoil existing the low-drag pocket regime where the drag decreases with the increase of angle of attack, this paper modifies the formula (4) based on test data from the DU97-W300-flatback airfoil[13]. The modified expression of the base drag coefficient is presented in Eq.(5), and the curve illustrating the change in drag coefficient is depicted in Figure 2(a). Furthermore, the modified estimation formula is verified using the FX77-W-343 airfoil[14] as shown in Figure 2(b). The results demonstrate that the modified base drag prediction formula aligns with the expected outcomes, thereby enhancing the accuracy of drag prediction in the optimization process.

$$\Delta C_{dbase} = 0.135\cdot h^{4/3} / (32\bullet C_d^{1/4} - 124 C_d^{1/2} + 290 C_d) \tag{5}$$

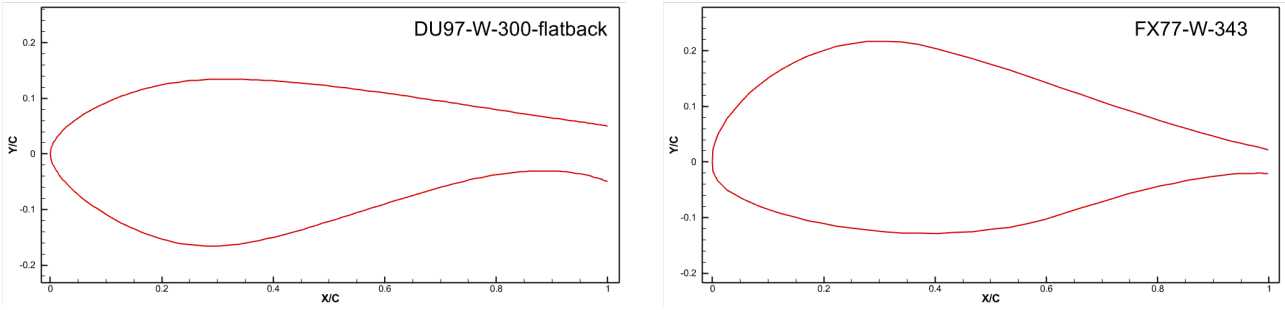

Figure 1 Airfoil geometry profile of the test case

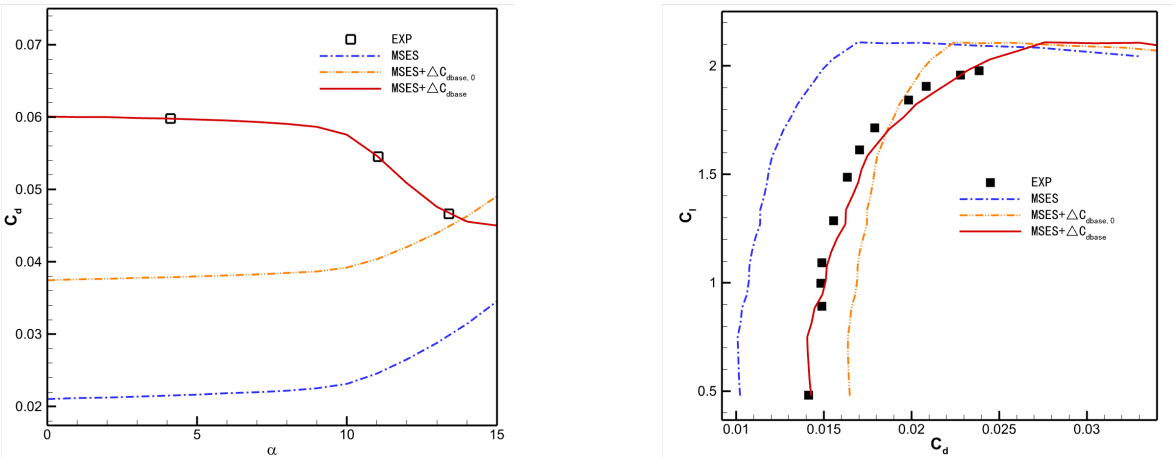

(a)DU97-W-300-flatback (b)FX77-W-343

Figure 2 Validation for thick airfoils' drag coefficient

2.2.2 Structural Performance Evaluation Methods and Validation

At present, the typical structural arrangement design method in wind turbine blade design is the double shear web design. The cross-section structure primarily consists of four parts: the main spar, the core plate, the shear-resistant web, and the leading edge and trailing edge reinforcements[15]. In this paper, the stiffness characteristics of an airfoil section with a chord length of 1m are evaluated using the open-source program PreComp (https://www.nrel.gov/wind/nwtc/precomp.html), with the layup design based on reference[16]. The program utilizes a modified version of the classical plywood theory to efficiently and accurately calculate the stiffness and inertia characteristics of composite blades. To validate the program's accuracy, a thin circular example with a theoretical solution is employed. The circle has a diameter of 1 m and is constructed using a 0.6 mm thick gelcoat ply. The equations for the cross-sectional moment of inertia and cross-sectional stiffness in all directions are presented in Eq. (6) and Eq. (7) respectively. A comparison between the calculated values and theoretical solutions is shown in Table 1, demonstrating good agreement and confirming the precision of the Precomp software in evaluating the stiffness characteristics of the cross-section.

$$I_{xx} = I_{yy} = \frac{\pi D^4}{64}(1-\alpha^4), I_p = \frac{\pi D^4}{32}(1-\alpha^4), \alpha = \frac{d}{D} \tag{6}$$

$$EI_x = E_1 \cdot I_{xx}, EI_y = E_2 \cdot I_{yy}, EI_Z = G_{12} \cdot I_P \tag{7}$$

Table 1 Comparison table for evaluating the stiffness of thin circular ring sections

	$EI_x(/10^5)$	$EI_y(/10^5)$	$EI_z(/10^5)$
theoretical value	8.0907	8.0907	6.4914
calculated value	8.091	8.091	6.490

2.2.3 High-fidelity numerical evaluation methods and validation

Considering that the accuracy limitation of the rapid aerodynamic performance evaluation method used in the optimization design in predicting the aerodynamic characteristics of airfoils with large blunt trailing edge separation flow, this paper employs a high-fidelity IDDES method to compare the aerodynamic characteristic of the optimized airfoil and the baseline. In this chapter, the reliability of the adopted IDDES method is verified by means of the large thickness flatback airfoil DU97-W300-flatback[13] example, which belongs to the DU series of airfoils with a maximum relative thickness of 30% and a dimensionless trailing edge thickness of 10%, the Reynolds number of experiment is 3.0×10^6. This example is one of the commonly used reference examples in numerical simulation analysis of large thickness flatback airfoils.

The adopted grid topology type is O-type. The height of the first layer of the grid is 8×10^{-6}m to satisfy the requirement of y+ < 1. The far-field distance is 100 times the chord length to avoid interference from the far-field boundary conditions on the computational results. The aspect ratio is 1 to guarantee

the full development of the spreading flow. The resulting number of the structured grids are 481 × 149 × 129. Additionally, to capture the tail vortex more finely, a nested grid is equally refined within the rectangular region from (0.5, -0.3, -0.5) to (2.5, 0.7, 0.5), bringing the final total number of grids to about 12 million. The grid schematic near the airfoil is shown in Figure 3.

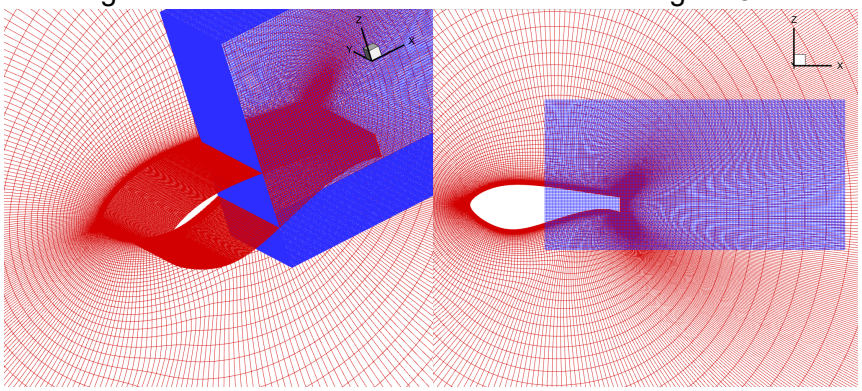

Figure 3 Airfoil grids used for simulation (DU-97-W300-flatback)

The results were evaluated when the simulation results converged well, as shown in the shaded area in Figure 4. Comparisons of the final calculated aerodynamic coefficients with the experimental values are shown in Table 2, Table 3 and Figure 5. From these comparisons, it can be seen that the IDDES method can predict the trend of the drag coefficient of the flatback airfoil decreasing with the increase of the angle of attack. The maximum error of the force coefficients is around 10%, indicating that the method is capable of reasonably predicting the aerodynamic characteristics of flatback airfoils with large thickness. This verifies the reliability of the hybrid RANS/LES method used.

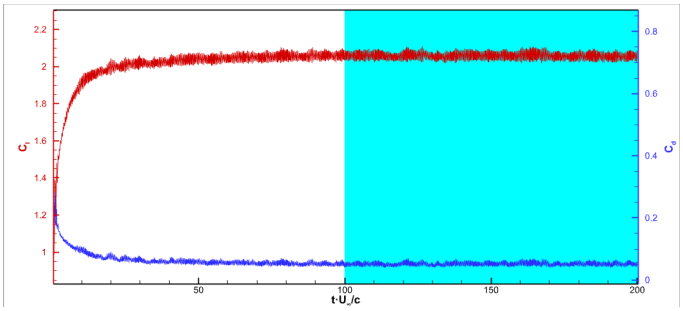

Figure 4 Convergence plot of force coefficients at α=13.4°

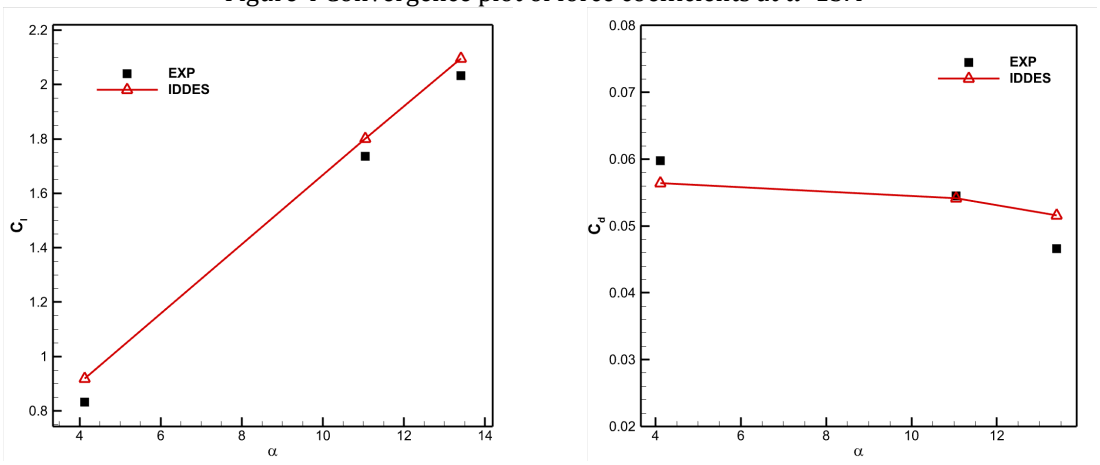

(a) Comparison of lift coefficients (b) Comparison of drag coefficients

Figure 5 Comparison of aerodynamic coefficients calculated by IDDES method with experimental values

Table 2 Comparison of lift coefficients calculated by IDDES method with test values

angle of attack	experimental value	simulation value	relative error
4.12°	0.833	0.9179	10.19%
11.05°	1.736	1.8013	3.76%
13.4°	2.033	2.0962	3.11%

Table 3 Comparison of drag coefficients calculated by IDDES method with test values

angle of attack	experimental value	simulation value	relative error
4.12°	0.0598	0.0564	-5.69%
11.05°	0.0545	0.0541	-0.73%
13.4°	0.0466	0.0516	10.70%

2.3 Numerical optimization framework

The mathematical model of a multi-objective optimization problem is generally shown in equation(8). In this paper, we use the Surrogate-Based Multi-Objective Optimization (SBMO) algorithm[17] proposed by our group to conduct the aerodynamic/structural multi-objective design optimization. The method first adopts the design of experiments (DoE) method to select initial sample points within the design space, and then performs numerical analysis to obtain the response values of the objective functions and constraint functions. Subsequently, multiple surrogate models for each optimization objective and constraint are established based on the sample data set. Using the Chebyshev decomposition method constructs sub-problems. New sample points obtain by infill-sampling. Evaluate new sample points and use the vaules to update the agent model until the optimization converges.

$$\begin{aligned} \min. \quad & F_1(x), F_2(x), \cdots, F_q(x) \\ s.t. \quad & g_i(x) \geq 0, \quad i=1,2,\cdots,m \end{aligned} \tag{8}$$

Figure 6 illustrates the design optimization framework presented in this paper. The process begins with generating the sample points using the 8th-order CST parameterization method. Subsequently, the aerodynamic and structural performance response values are calculated using MSES with base drag modification and PreComp software. Based on these calculations, a corresponding mathematical model is constructed utilizing the self-developed optimizer "SurroOpt" by the research group, which employs a surrogate optimization algorithm to build the mathematical model and generate new sample points for iterative cycles. This process continues until the convergence criterion of the optimization design is satisfied. Ultimately, a Pareto frontier that comprehensively considers both aerodynamic and structural performance is obtained.

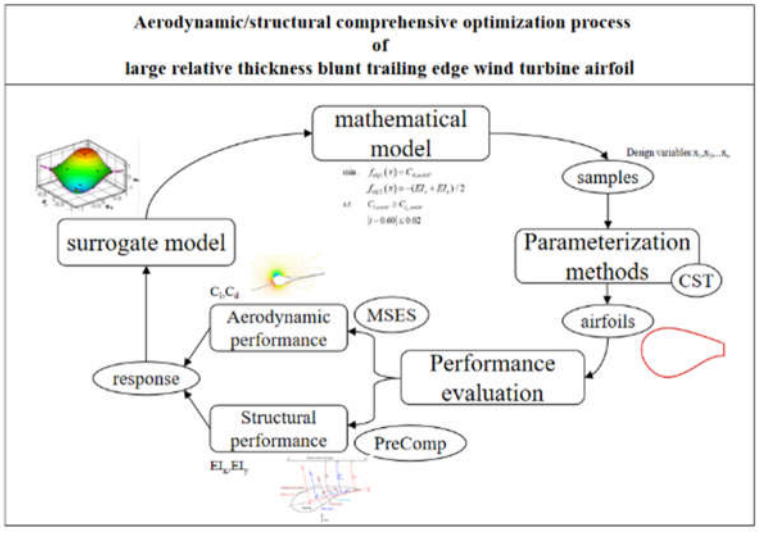

Figure 6 Design optimized process for large thickness flatback airfoils

3. Results and Discussions

3.1 Optimization Results

The aerodynamic and structural multi-objective optimization design is conducted, the large thickness flatback airfoil NPU-MWA-600[18], which is designed by Northwestern Polytechnical University is used as the baseline. NPU-MWA-600 airfoil's relative thickness is 60%, and the trailing edge thickness is 15%. It has excellent structural and aerodynamic characteristics, good geometric and aerodynamic

compatibility with other airfoils in the NPU-MWA airfoil family (Figure 7), as illustrated by its geometric shape in Figure 8

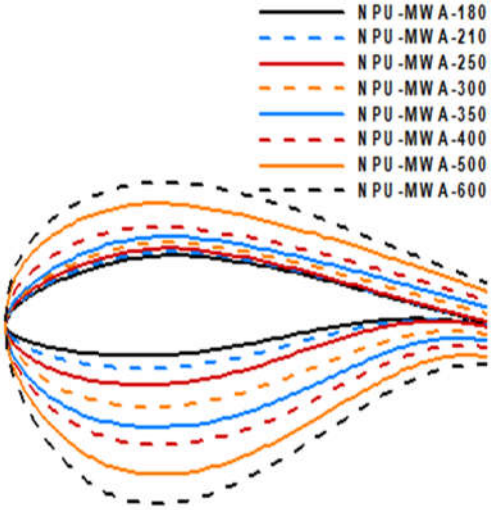

Figure 7 NPU-MWA airfoil family

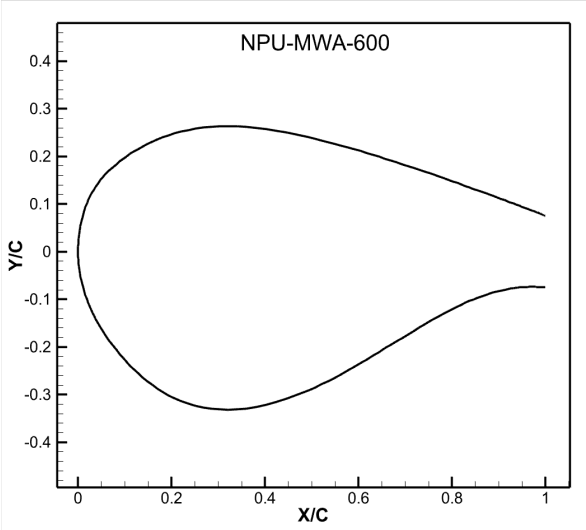

Figure 8 NPU-MWA-600 Geometric Profile

The optimization problem of this paper is shown in Eq.(9), where 'C_l' and 'C_d' are the lift coefficient and drag coefficient of the airfoil, 'EI_x' and 'EI_y' represent the cross-section stiffness in the flapwise and edgewise directions, ' t' is the maximum relative thickness of the airfoil, and the subscript 0 represents the performance parameter of the baseline. The design state is Ma=0.267，$Re=6\times10^6$，α=14°, and the design space is shown in Figure 9.

$$\begin{aligned} \min. \quad & f_{obj1}(x) = C_d / C_{d,0} \\ & f_{obj2}(x) = -(EI_x / EI_{x,0} + EI_y / EI_{y,0}) / 2 \\ s.t. \quad & C_l \geq C_{l_0} \\ & |t - 0.60| \leq 0.02 \end{aligned} \tag{9}$$

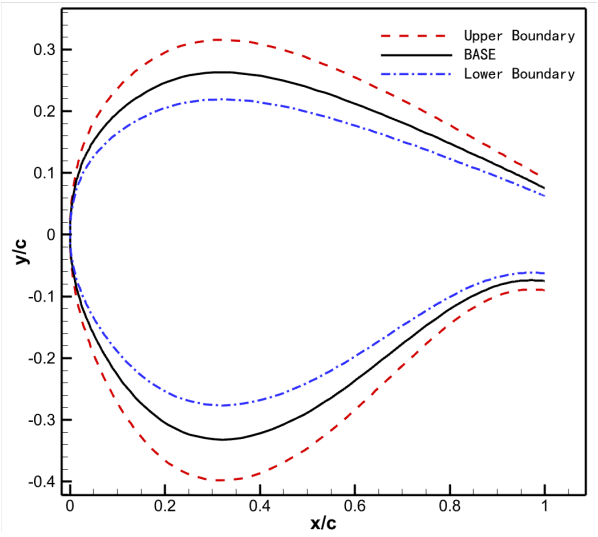

Figure 9 Design space for design optimization

Figure 10 demonstrates the normalized Pareto leading edge, and three typical airfoils are selected, which are named as OPT1, OPT2 and OPT3 according to the structural strength in descending order, and the geometries of the optimized airfoils and the baseline are shown in Figure 11, the detailed information of the profile parameters and structural stiffnesses are shown in Table 4 and Table 5.

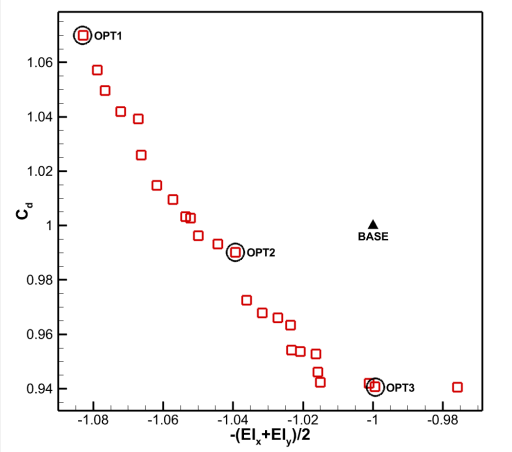

Figure 10 Pareto frontier diagram

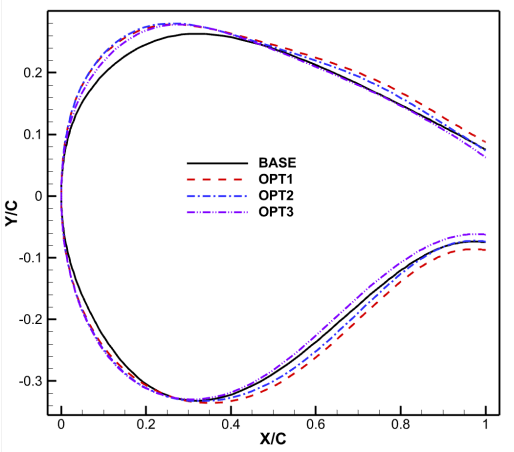

Figure 11 Airfoils geometry profile comparison

Table 4 Comparison of airfoil geometrical parameters before and after optimization

	baseline	Opt1	Opt2	Opt3
Leading edge radius/chord	28.2%	40.6%	40.5%	37.3%
thickness/chord	59.48%	60.51%	60.96%	60.67%
maximal thickness position	32%	30.7%	30.3%	29.3%
camber/chord	1.59%	1.84%	1.9%	2.0%
maximal camber position	86.40%	86.0%	86.0%	84.6%
trailing edge thickness/chord	15%	18%	14.7%	12.5%
Area	0.412	0.445	0.434	0.414

Table 5 Comparison of airfoil structural stiffness before and after optimization

	$EI_x(/10^8)$	$EI_y(/10^8)$	$EI_z(/10^7)$
baseline	1.090	2.515	2.525
Opt1	1.223(+12.2%)	2.681(+6.6%)	2.928(+16.0%)
Opt2	1.202(+10.3%)	2.592(+3.1%)	2.762(+9.4%)
Opt3	1.133(+3.9%)	2.506(-0.4%)	2.512(-0.5%)

From the comparison table, it can be seen that for the three optimized airfoils, the change in trailing edge thickness has the most significant effect on structural performance. Increasing the trailing edge thickness effectively increases the airfoil's cross-sectional area and structural stiffness in all directions, providing a notable structural performance advantage. Additionally, the radius of the leading edge in the optimized airfoils is significantly larger than that of the baseline. This increase in radius also contributes to the greater cross-sectional area and structural strength, particularly enhancing the flapwise direction stiffness.

3.2 Aerodynamic characteristics Comparisons by High-fidelity IDDES method

To accurately analyze the factors influencing the aerodynamic performance of large-thickness flatback airfoils, this paper conducts a detailed evaluation using the high-fidelity IDDES method. The computational conditions include Ma = 0.267 and Re = 6×10^6. The first layer height of the grid is set to 4×10^{-6} times of the chord length to ensure y+<1. The wake region is defined by a modified rectangular enclosure from (0.5, -0.5, -0.5) to (2.5, 0.5, 0.5), while other parameters remain consistent with those described in Section 2.2.3. Figure 14 illustrates the grid configuration.

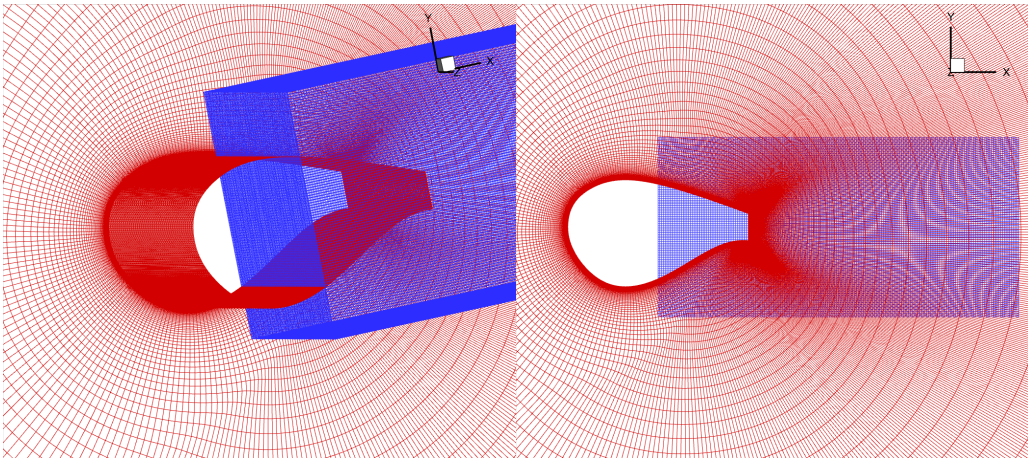

Figure 12 Airfoil grids used for simulation (NPU-MWA-600)

For the design state α = 14°, the convergence curves of the calculated aerodynamic coefficients over 100 cycles are shown in Figure 13, and the comparisons of the aerodynamic coefficients are shown in Table 6. It can be seen that the lift-resistance characteristics of the OPT1 and OPT2 airfoils are significantly better than those of the baseline and OPT3, and the convergence of the aerodynamic coefficients is also significantly better, which is analyzed to be caused by the difference in their stall characteristics.

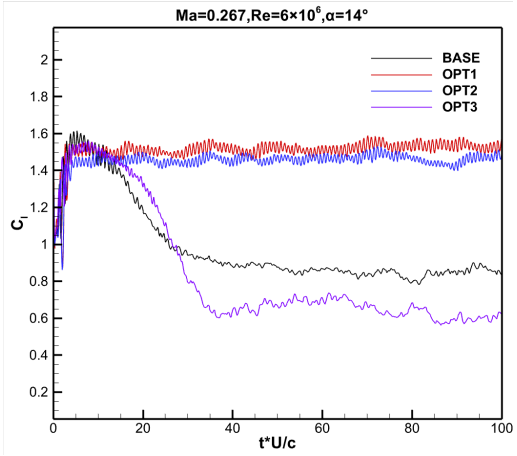

(a) Lift coefficient convergence curve

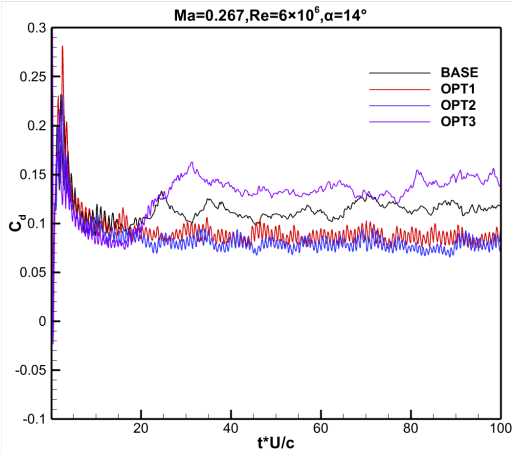

(a) Drag coefficient convergence curve

Figure 13 Convergence curve of aerodynamic coefficients at design state

Table 6 Comparison of aerodynamic performance before and after optimization

	C_l	C_d	C_l/C_d
baseline	0.848	0.1157	7.33
Opt1	1.527(+80.07%)	0.0868 (-24.98%)	17.59
Opt2	1.454(+71.46%)	0.0766(-33.79%)	18.98
Opt3	0.605(-28.65%)	0.1450(+25.32%)	7.17

By observing the vorticity diagram (Figure 14) and the flow field diagram (Figure 15), it can be seen that the separation position of the suction surface of the baseline airfoil and OPT3 airfoil is forward, which is seriously affected by vortex shedding, resulting in the inability to exert the excellent aerodynamic performance when it is not stalled. On the other hand, the flow separation of the suction surface of the OPT1 and OPT2 airfoils is significantly suppressed, and the stall characteristics are relatively good. The comparison of the geometrical profiles (Figure 11) shows that the suction surface of the OPT1 and OPT2 airfoils has an obvious bulge in the region of 40% chord length to 90% chord length compared with the baseline airfoils, which leads to a gentle change in the suction surface profiles, thus suppressing the flow separation and improving the stall characteristics of the airfoils.

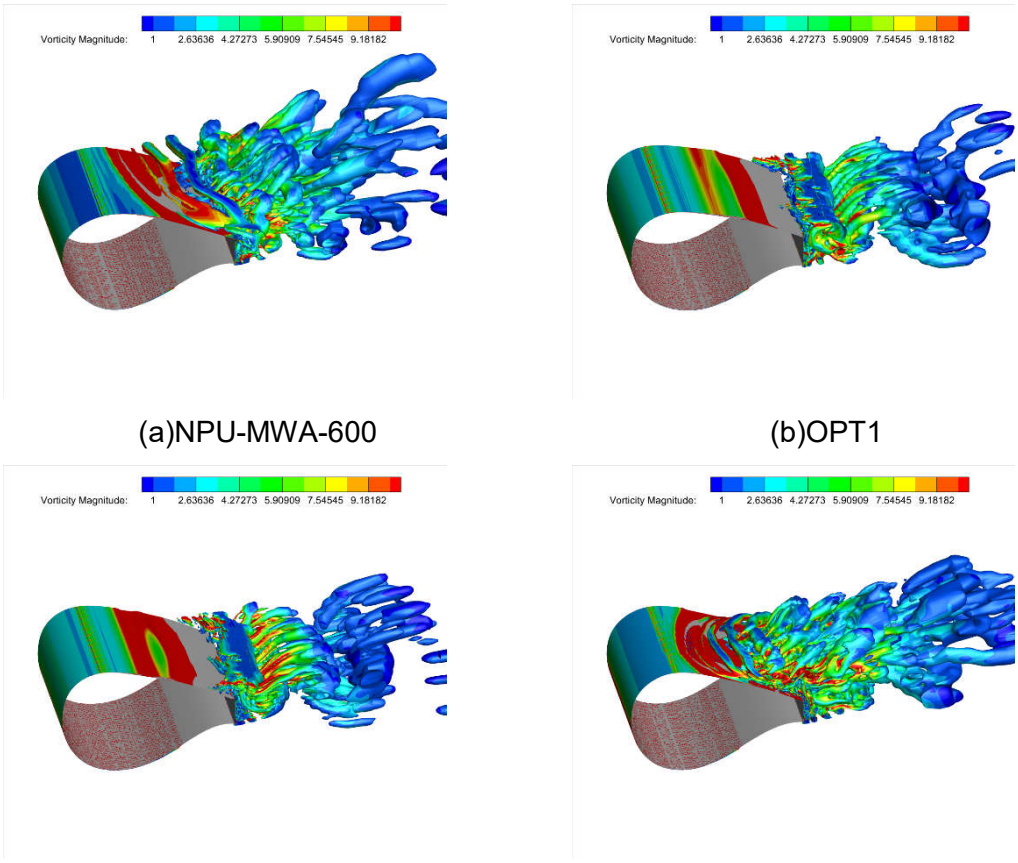

(a)NPU-MWA-600 (b)OPT1

(c)OPT2 (d)OPT3

Figure 14 Vorticity diagram at design state

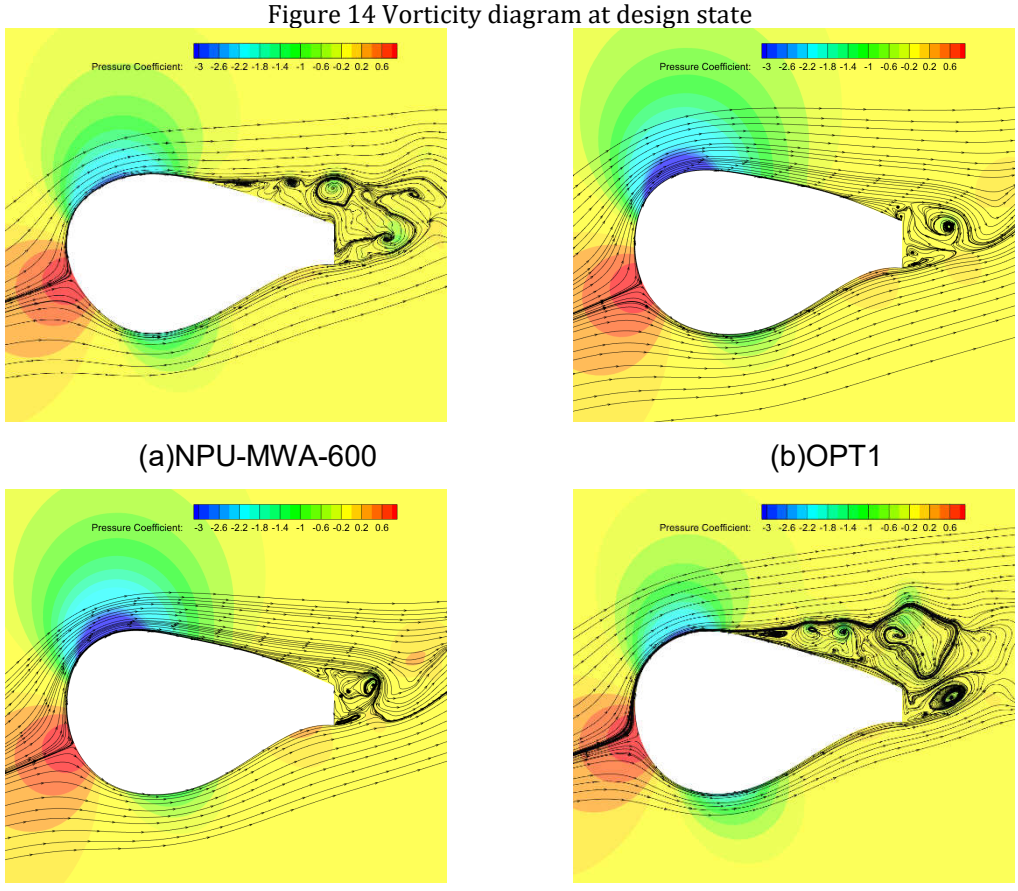

(a)NPU-MWA-600 (b)OPT1

(c)OPT2 (d)OPT3

Figure 15 Flow field diagram at design state

In addition, comparing the aerodynamic characteristics of the OPT1 and OPT2 airfoils, it can be seen

that the OPT1 has a larger lift coefficient and drag coefficient but a lower lift-to-drag ratio, a phenomenon that may be related to the trailing edge thickness. The larger thickness of the trailing edge of the OPT1 airfoil better inhibits the separation flow on the suction surface and improves the lift characteristics, but at the same time it also brings about stronger shedding vortices, resulting in an increase in drag. The trailing edge thickness of the OPT2 airfoil is relatively moderate, which better balances the contradiction between the lift and drag characteristics, and ultimately has a higher lift-to-drag ratio.

The comparison of the aerodynamic coefficient curves for each airfoil at various angles of attack is depicted in Figure 16. The figure illustrates that, below a 10° angle of attack, the optimized airfoils exhibit poorer lift-drag characteristics compared to the benchmark airfoils. However, beyond a 10° angle of attack, the benchmark airfoils gradually enter a stalled state, whereas the OPT1 and OPT2 airfoils demonstrate improved stall characteristics, resulting in higher lift coefficients and lift-drag ratios at higher angles of attack. This characteristic enables them to better accommodate the operational requirements of the root airfoils in wind turbine blades when subjected to large angles of attack.

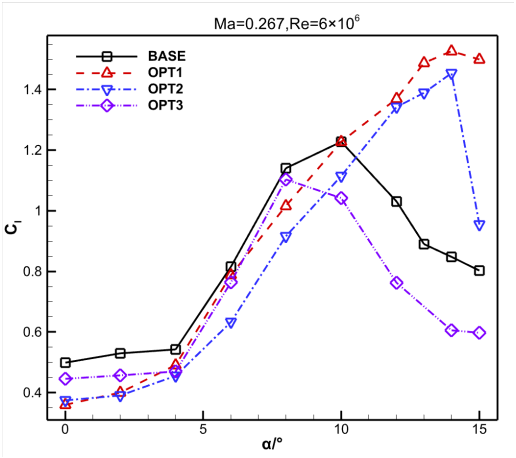

(a) Lift coefficient comparison curve

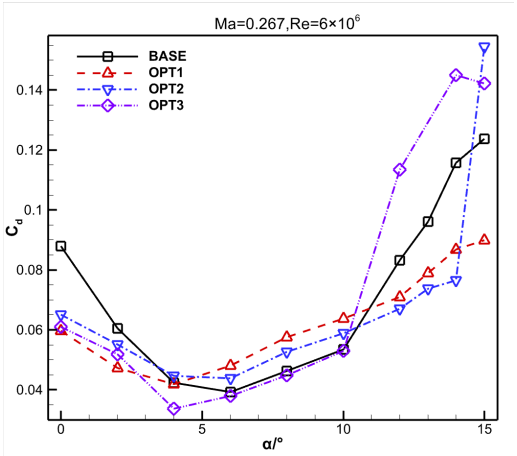

(a) Drag coefficient comparison curve

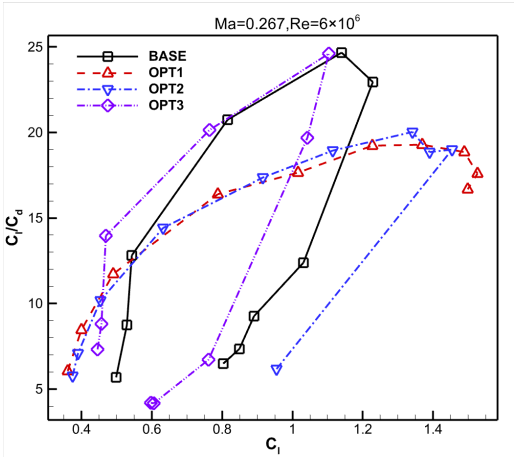

(c) Lift-drag ratio comparison curve

Figure 16 Comparison curve of aerodynamic coefficient at different angles of attack

Furthermore, the relationship between the aerodynamic coefficients of each airfoil and the angle of attack reveals that angles of 0° and 2° do not fall within the linear segment of the lift coefficient, resulting in higher drag coefficients. This behavior is primarily attributed to the presence of a separation vortex on the pressure surface. For instance, considering the benchmark airfoil, vortex diagrams at different angles of attack are presented in Figure 17. At a 0° angle of attack, evident flow separation occurs on the airfoil's pressure surface, gradually diminishing as the angle of attack increases, ultimately leading to the suppression and disappearance of the separation vortex. Consequently, the drag coefficient initially decreases before rising again, reflecting this aerodynamic phenomenon.

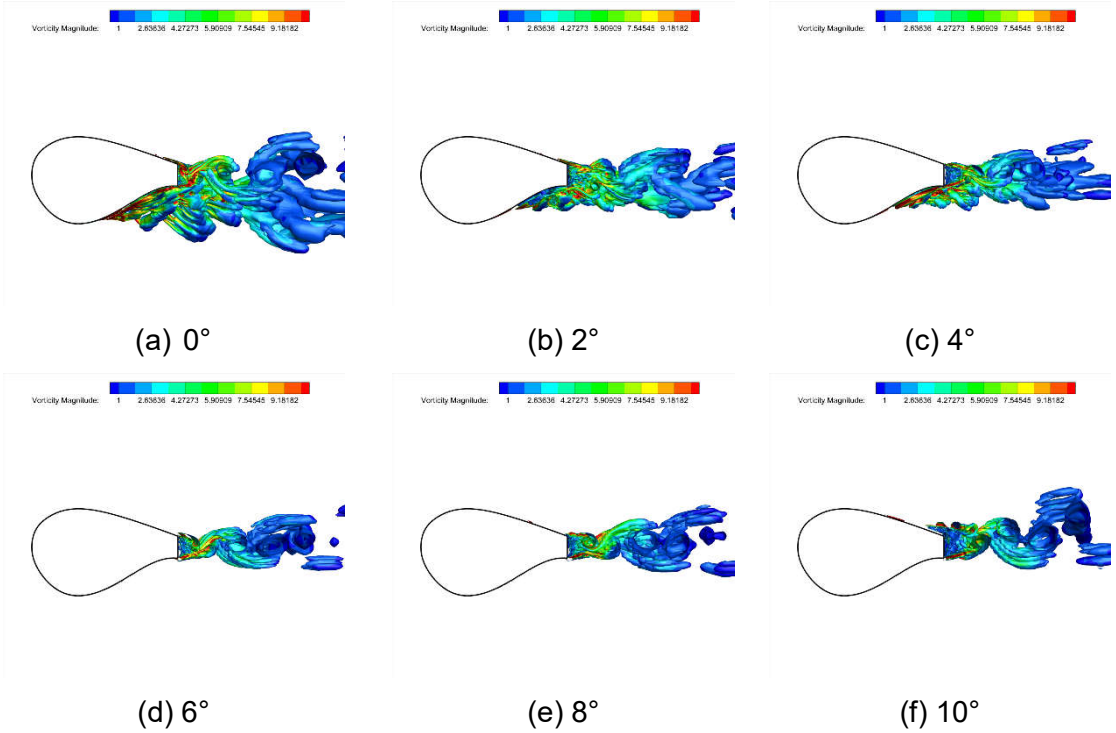

(a) 0° (b) 2° (c) 4°

(d) 6° (e) 8° (f) 10°

Figure 17 Vortex variation at different angles of attack of the baseline

4. Conclusion

In this paper, to meet the structural and aerodynamic performance requirements of ultra-large wind turbine blades, a multi-objective design optimization method for large-thickness flatback airfoils that accounts for both aerodynamic and structural requirements is developed. Using the aerodynamic and structural design optimization of a flatback airfoil with a relative thickness of 60% as an example, a set of 25 optimal shapes forming the Pareto solution set is obtained. The aerodynamic characteristic comparison of the optimized airfoil and the baseline is carried out by using a high-fidelity IDDES method. The conclusions are as follows:

(1) This paper develops a base drag correction formula, which can effectively predict the variation trend of drag for large thickness flatback airfoils.

(2) The optimization design method developed in this paper can effectively carry out the trade-off design of aerodynamic/structural performance for large thickness flatback airfoils. The optimized airfoils on the Pareto front can be selected by designers for blade design, based on the radial position of the airfoil on the blade, to emphasize aerodynamic performance, structural performance, or a balance of both.

(3) This paper uses the high-fidelity IDDES method to compare the aerodynamic characteristics of the optimized airfoils and the baseline airfoil. It was found that the elevation of the mid-to-aft section (40%-90%) of the suction surface effectively suppresses flow separation at high angles of attack for large thickness flatback airfoils, increasing the stall angle of attack.

5. Acknowledgment

This work is funded by the National Key R&D Program of China (No. 2020YFB1506703). The work was carried out at National Supercomputer Center in Xi'an, and the calculations were performed on Sugon.

6. Contact Author Email Address

Wen-Ping Song *, wpsong@nwpu.edu.cn, corresponding author.

7. Copyright Statement

References

[1] Global Wind Report 2023-Annual Market Update. https://gwec.net/globalwind report2023.

[2] LI Limin. Has the era of large-scale offshore wind turbine come. [N]. China Energy News, 2021-08-23(9).

[3] 143 meters! The world's longest wind turbine blade rolls off the production line. https://news.bjx.com.cn/ html/20240228/ 1363213.shtml.

[4] Standish K J, van Dam C P. Aerodynamic analysis of blunt trailing edge airfoils [J]. Journal of Solar Energy Engineering-Transactions of the ASME, 2003, 125(4): 479—487.

[5] Kahn D L, Van Dam C P, Berg D E. Trailing edge modifications for flatback airfoils[R]. SAND 2008. 1781. 2008.

[6] Park H. Drag Reduction in Flow over a Two-dimensional Bluff Body with a Blunt Trainling Edge using a New Device. J Fluid Mech,2006,563:389—414.

[7] Standish K J，van Dam C P. Aerodynamic analysis of blunt trailing edge airfoils[J]. Journal of Solar Energy Engineering-Transactions of the ASME, 2003, 125(4): 479-487.

[8] Kahn D L, Van Dam C P， Berg D E. Trailing edge modifications for flatback airfoils[R]. SAND 2008.1781.2008.

[9] Kulfan B M. A universal parametric geometry representation method – ‘CST’. AIAA-2007-62, 2007.

[10]M. Drela, M.B. Giles, Viscous-inviscid analysis of transonic and low Reynolds number airfoils, AIAA J. 25 (10) (1987) 1347–1355, https://doi.org/10.2514/ 3.9789.

[11]F. Grasso. Modeling and Effects of Base Drag on Thick Airfoils Design. 32nd ASME Wind Energy Symposium, 2014

[12]Hoerner, S.F., “Base Drag and Thick Trailing Edge”. Journal of the Aeronautical Sciences, Vol. 17, No. 10, Oct. 1950, pp. 622-628.

[13]M. Barone, D. Berg. Aerodynamic and Aeroacoustic Properties of a Flatback Airfoil: An Update[C]. 47th AIAA Aerospace Sciences Meeting Including The New Horizons Forum and Aerospace Exposition, 2009: 1-14.

[14]Anon. “UIUC Airfoil Coordinates Database,” UIUC Applied Aerodynamics Group, University of Illinois Urbana-Champaign, Department of Aerospace Engineering, [Online], http://m-selig.ae.illinois.edu/ads/coord_database.html

[15]Giunta, A. A., Wojtkiewicz, S. F. Jr., and Eldred, M. S., Overview of modern design of experiments methods for computational simulations[C], AIAA 2003-649, 6–9 January 2003.

[16]WANG Q, CHEN X T, HU M J, et al. Optimization Design of Wind Turbine Airfoils Based on Aerodynamic Performance and Stiffness Characteristics[J]. China Mechanical Engineering, 2020, 31(19): 2283-2289.

[17]Han Z H, Xu C Z, Qiao J L, et al. Recent progress of efficient global aerodynamic shape optimization using surrogate-based approach [J]. Acta Areonautica et Astronautica Sinica, 2020, 41(5):623344

[18]Han Z H, Song W P, Xu J H, et al. A series of airfoils suitable for 5-10 MW wind turbine blades. CN201610164779. X [P]. 2016-08-10.